JAAS

Accepted Manuscript

This is an *Accepted Manuscript*, which has been through the Royal Society of Chemistry peer review process and has been accepted for publication.

Accepted Manuscripts are published online shortly after acceptance, before technical editing, formatting and proof reading. Using this free service, authors can make their results available to the community, in citable form, before we publish the edited article. We will replace this *Accepted Manuscript* with the edited and formatted *Advance Article* as soon as it is available.

You can find more information about *Accepted Manuscripts* in the Information for Authors.

Please note that technical editing may introduce minor changes to the text and/or graphics, which may alter content. The journal's standard Terms & Conditions and the Ethical guidelines still apply. In no event shall the Royal Society of Chemistry be held responsible for any errors or omissions in this *Accepted Manuscript* or any consequences arising from the use of any information it contains.

ROYAL SOCIETY OF CHEMISTRY

www.rsc.org/jaas

A metric for evaluation of the image quality of chemical maps derived from LA-ICP-MS experiments

*Maximilian Bonta[1], Andreas Limbeck[1], C. Derrick Quarles, Jr.[2], Dayana Oropeza[3], Richard E. Russo[2,3], and Jhanis J. Gonzalez[2,3]**

[1]Vienna University of Technology, Institute of Chemical Technologies and Analytics, Vienna, Austria
[2]Applied Spectra, Inc., Fremont, CA
[3]Lawrence Berkeley National Laboratory, Environmental Energy Technologies Division, Berkeley, CA

Abstract

For laser ablation-inductively coupled plasma-mass spectrometry (LA-ICP-MS) imaging experiments – as well as other techniques used for elemental or molecular mapping – the accordance of the measured distribution with the actual distribution is of utmost importance to guarantee reliability of the obtained images. In most experiments reported in the past, the experimental conditions have been chosen so that washout effects and signal carry-over are minimized by scanning the sample surface very slowly. Therefore, measurement times become very long and decently resolved images will require acquisition times of several hours up to more than one day. To increase the application range of LA-ICP-MS for imaging it is important to decrease the measurement times, which is best accomplished by increasing the scanning rates. However, depending on the instrumentation, this can lead to blurring and compromised image quality. In this work, we present a metric to compare the measured elemental distribution with their actual distribution based on a sample with visually distinguishable features. This approach allows quantitative determination of the image quality and enables comparison of multiple measurement conditions. This information can be used for method optimization, to get a reasonable tradeoff between image quality and measurement time.

Introduction

Laser ablation-inductively coupled plasma-mass spectrometry (LA-ICP-MS) has gathered interest in various fields of science during the past decades[1-6]. The opportunity to perform laterally resolved analyses combined with sub-µg g^{-1} detection limits for most elements using modern ICP-MS instrumentation is valuable for addressing a large range of scientific applications. Besides the use of LA-ICP-MS for bulk analysis, circumventing the problem of complex and time consuming sample preparation, this technique is also frequently utilized for elemental mapping (imaging) of samples in two or three dimensions[7]. Typically, imaging experiments are employed for mapping of elements in minerals[8, 9], biological materials[10-14], and other sample types[15]. Typical lateral resolutions range between 20 and 100 µm. Recent achievements in LA-ICP-MS imaging, especially involving bio-imaging, have lead to improved lateral resolutions down to 1 µm[16, 17].

A challenge for LA-ICP-MS imaging measurements is to reduce the long acquisition time required for these experiments. Depending on the desired lateral resolution and sample area, some measurements may take up to 30 hours or more[18], making this technique laborious for routine analyses especially if fast sample throughput is required. Typically, two approaches are used for imaging experiments with LA-ICP-MS. The first one is a spotscan over the sample surface. The laser is systematically fired onto discrete spots subsequently covering the whole region of interest on the sample. Typical waiting times between

*Corresponding author. **Tel:** 510-4952899, **Fax:** 510-4867303, **Email:** jjgonzalez@lbl.gov

two spots are from microseconds to a few seconds (0.1-10 s, depending on the cell volume) to ensure total particulate washout from the cell. Certainly, this method allows for the most reliable imaging by avoiding image blurring. However, a long measurement time is required for complete aerosol washout from the chamber. The second and more often employed method[18, 19] uses linescans covering the area of interest on the sample. Using the desired laser beam diameter, line after line is scanned and the recorded signals are either saved as one file or as single files for every line, depending on the software or algorithm used for data evaluation and image construction. The crucial parameters of linescans are the laser repetition rate and the scan speed, both of which will influence the image quality of the resulting elemental maps. At a constant laser beam diameter, the total measurement time is determined only by the scan speed. In many experiments, laser scan speeds are set based on the laser beam diameter. Often, very slow scan speeds have been reported to be used. Still, compared to a spotscan, this approach drastically reduces the measurement time. Moreover, even higher scan speeds may be applied and still deliver a satisfactory image quality with further reduced measurement time, as stated in previous publications[20]. In both approaches, the material washout of the cell is important, and in this latest approach a slow washout combined with high scan speeds might lead to signal carryover to following sample locations leading to distortion of the image.

Already earlier, Lear *et al.*[20] investigated the effect of changing sampling parameters on image quality. It showed that fast scan speeds are applicable for imaging experiments, making the measurements more time efficient. However, it has been stated that the washout behavior of the used cell plays a significant role for the maximum obtainable scan speed and thus, image quality might suffer from blurring effects.

In this work, we present an approach for evaluation of the image quality in terms of correlation with a visual image of the sample. The correlation is described by a metric, to accurately determine the quality of the elemental distribution image. In contrast to previously presented studies with the goal to optimize imaging parameters, the aim of this study was the quantitative determination of the image quality. Metrics obtained from different images can be easily compared, without being influenced by the instrument where the measurement has been performed or the method of image construction. For method development, printed patterns on paper have been used, which have already been shown to be a valuable tool for evaluation of parameters in imaging experiments[21, 22].

Methods

Instrumentation

Experiments were performed using a femtosecond laser ablation instrument (J200, Applied Spectra Inc., Fremont, CA) coupled to an inductively coupled plasma mass spectrometer (Bruker Aurora elite, Bruker, Billerica, MA). The instrumental conditions were checked on a daily basis to ensure proper function of the instrumentation using the certified reference material NIST610 trace elements in glass (National Institute of Standards and Technology, Gaithersburg, MD). Typical instrumental parameters are shown in Table 1.

Table 1: Typical instrumental parameters used for the sample measurements

laser ablation		ICP-MS	
wavelength	1030 nm	plasma power	1500 W

pulse duration	450 fs	cool gas flow	18.0 $Lmin^{-1}$
laser repetition rate	10, 20, 40 and 80 Hz	auxiliary flow	1.8 $Lmin^{-1}$
laser beam diameter	40 µm	cones	Ni
laser energy	120 µJ	scanning mode	peak hopping
laser scan speed	0.05, 0.1, 0.2, 0.5 mms^{-1}	dwell time per isotope	8 ms
laser beam geometry	circular	monitored isotopes	^{13}C, ^{48}Ti, ^{63}Cu, ^{65}Cu
He gas flow	0.7 L min^{-1}	mass resolution	300 m/Δm
Ar make-up flow	0.7 L min^{-1}		

Ablation of the sample material was performed under a constant helium gas flow, which was subsequently mixed with argon as make-up gas using a glass T-piece in close proximity of the ablation chamber outlet. Helium gas flow was optimized in preliminary experiments to obtain the shortest possible washout times. Two different cell volumes (33 mL and 16 mL) were evaluated for washout effects. Both cells were of drop-shaped geometry with the in- and outlet positioned along the axis of symmetry. In this work, the cell with an inlet-outlet distance of 65 mm will be referred to as 'large cell' and the cell with a 45 mm inlet-outlet distance as 'small cell'. The described cells are commercially available standard equipment of the used laser ablation system. For measurement each sample was placed along the axis of symmetry one centimeter from the cell outlet.

Preparation of printed patterns

Printed patterns were designed in Microsoft Power Point 2010 (Microsoft Corp., Redmond, WA). Blue color (RGB color code #00FFFF) was used to design the patterns. Squares sized 200x200, 300x300 and 400x400 µm were drawn with distances between 200 and 400 µm between the edges of the squares. The patterns were printed using a conventional office laser printer (Brother, Nagoya, Japan) onto white office paper with a high resolution print setting (2400 dpi). After the printing process, single patterns were cut out and attached to microscopic glass slides using double sided tape. Each slide was equipped with only one pattern to ensure identical position of each sample in the ablation cell, since altered washout due to a changed sample position could affect the results of the measurements.

Processing of the visual images

The pigment from the blue color printed onto the paper samples contains copper; the background signal of copper from the paper was negligible in preliminary experiments. Signals for the copper background yielded around 5.000 cps (^{65}Cu), compared to more than 5.000.000 cps on areas with ink application. Therefore, the only considerable source of copper was the ink deposited on the paper. Before the LA-ICP-MS experiments, microscopic images of the samples were taken to enable comparison of the actual copper distribution (represented by the blue color) with the obtained copper distribution maps from the LA-ICP-MS analysis. The visual sample images were preprocessed to a size of 680x600 pixels, and maximum contrast was set to obtain the best visual differentiation between the blue color and the paper surface. Thereafter, the colored image was processed to a black and white image. Image preprocessing steps were performed using photographic image processing software (Adobe Lightroom 4.1, Adobe Systems, San Jose, CA). The resulting images were imported to Origin Pro 9.0 (OriginLab Corp., Northampton, MA) and processed to binary images consisting of only black and white pixels by setting a proper cutoff value between black and white; areas with ink deposition were white while areas without ink were black.

LA-ICP-MS measurement of the printed pattern samples and image construction

All measurements were performed with a laser beam diameter of 40 µm ablating a total sample area of 2.72 x 2.40 mm. The resulting distribution images were 68 x 60 pixels in size with each pixel covering 40 µm of the sample in both horizontal and vertical direction. In contrast to the other reported optimization study[20], the quadrupole dwell time was kept constant throughout all experiments, to show only the effects of altered laser sampling conditions on the image quality. Raw data were exported as text files and processed using ImageLab (Epina GmbH, Pressbaum, Austria). Spotscans were performed at a 20 Hz repetition rate firing 10 shots per location (0.5 s ablation time) with a 10 second delay between ablation of each location to let the signal reach background level after each laser shot. The distance between the centers of adjacent laser shots was 40 µm in both the horizontal and vertical directions.

Linescans were performed at varying laser repetition rates and laser scan speeds. All assumptions made here are valid when the whole sample is ablated during the analysis (i.e. for thin sections or thin films). The scan direction was kept constant for each line and the delay time between the ablation of two consecutive lines was 10 s. The signals of elements that are constituents of the paper were used for automatic detection of the measured lines using ImageLab[23]. The values for the horizontal pixels were calculated by dividing the signals obtained for the lines into 68 regions, such that every pixel spans 40 µm in horizontal direction. The acquired data points in each one of those regions were averaged to calculate the pixel values for the distribution images. A virtual sample (Figure 1a) is scanned using two different laser scan speeds. The data treatment for image construction is illustrated in Figure 1b and c. In this example the laser beam diameter is 40 µm. The regions are set such that the laser beam covers 40 µm in the length of one region; 1.0 s for 0.040 mm s^{-1} and 0.25 s for 0.160 mm s^{-1}, respectively. The intensity averages of the raw signals recorded in each of those regions deliver the pixel values for one horizontal line. When using higher scan speeds the time one region spans gets shorter as the laser covers more distance in the same amount of time. As the washout of the cell is independent from the scan speed more pixels will have wrong values than at slower scan speeds. The illustration in Figure 1 shows that higher scan speeds promote blurring effects. While in Figure 1b (40 µm s^{-1}) only one region (pixel) is affected by the washout, Figure 1c shows at least 4 pixels will represent wrong signal intensities before the signal intensity reaches background level again.

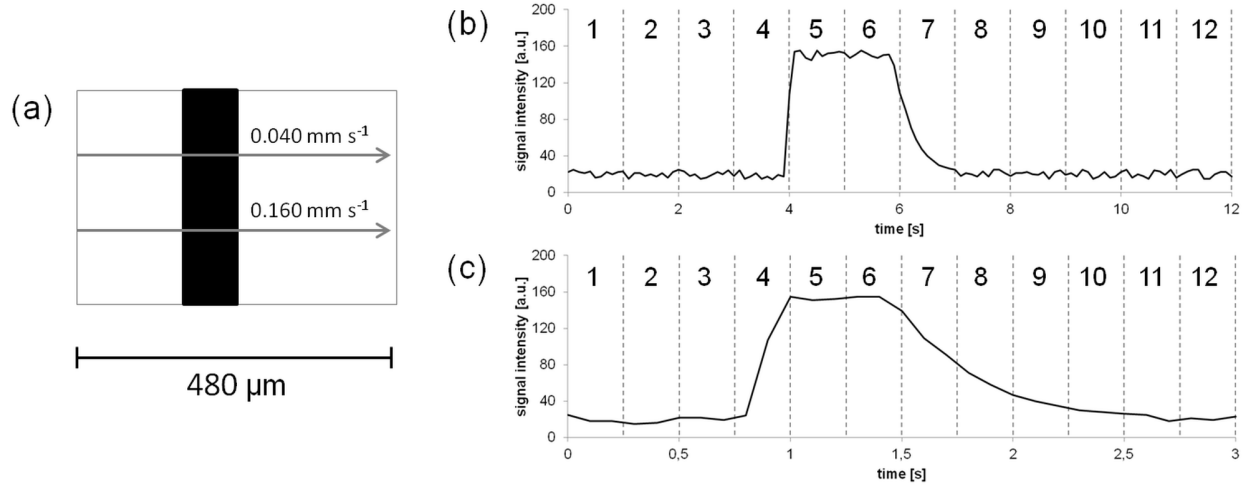

Figure 1: Illustration of a virtual sample with an 80 µm wide feature containing an arbitrary element (feature in black, (a)), simulated ICP-MS signals for the same element for the scan speeds 40 µm s^{-1} (b) and 160 µm s^{-1} (c) with the numbered regions for calculation of the pixel intensities

For both spot- and linescans, time resolved data were acquired and stored in a single file. The largest squares of the printed pattern (400 x 400 µm) were used to calculate the reference value for the detection threshold. This value was determined using the average intensity of ^{65}Cu at the center of these squares (3 x 25 pixels). Using the 10 percent valley definition commonly used in mass spectrometry to determine peak separation[24], a signal drop of 90% was regarded as being sufficient evidence that no major blurring effects would occur. Binary distribution images of ^{65}Cu were calculated with white areas representing the presence of a ^{65}Cu signal above the calculated threshold and black areas showing signal intensities below this mark. Matching of the elemental distributions with the visual image was accomplished using the knowledge of the exact position of the ablated area.

Comparison of the binary images

For each analyzed sample, two binary images were created. One shows the presence of copper represented by the blue color in the light microscopic image, and the other shows if a ^{65}Cu signal 10% above the average maximum signal has been detected using LA-ICP-MS. To expose the areas that are similar or different, the two images were treated as matrices and a simple subtraction step was performed. As the two images were initially of different resolution (the resolution of the visual image is typically higher than the one of the elemental image), the image sizes had to be adjusted in order to carry out the subtraction. Therefore, the size of the elemental image was expanded to fit the size of the visual image. If the size of the visual image is an integral multiple of the size of the elemental image this expansion can be performed without interpolation of pixels, i.e. pixels of one color divided into more pixels of the same color. When processing the visual image, this aspect has to be considered, and the final visual image has to fulfill this requirement. The process of image resizing is illustrated in Figure 2.

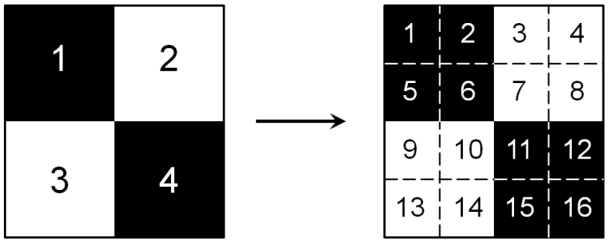

Figure 2: Illustration of the image expansion from a 2x2 pixel image matrix to a 4x4 image matrix

After the adjustment of the image dimensions, the values of corresponding pixels in the two images can be subtracted. This may result in two different scenarios: both pixels are either white or black, therefore the result of the subtraction will equal zero; or one of the pixels is black and one is white, so the result of the subtraction will be different from zero. If the result of the subtraction is zero, pixels are matching; if the result is unequal to zero pixels are not matching. Therefore, the amount of pixels with a value other than zero can be used as a measure for the area that has been wrongly assigned in the elemental image. A value describing the amount of mismatched areas (area mismatch percentage, AMP) can further be calculated as a percentage of the wrongly assigned area and the total image area. This metric can be used to describe the image quality of each measured elemental distribution image. It has to be pointed out, that after expansion of the initial elemental distribution image the term pixel is no longer referring to the actual lateral resolution of the map but is just used as an area measure.

Results and discussion

Measurement time and optical image comparison

As pointed out earlier, the long measurement time of LA-ICP-MS is a point of concern for the application of this technique for a broader range of imaging applications. Sample throughput can be increased and resources such as gas and electricity can be saved by making imaging analyses using LA-ICP-MS faster. The investigation of the samples presented in this work takes about 12 hours using a spotscan with a 10 s waiting time between the ablation of two adjacent spots. The analysis time can be drastically reduced using linescans (even with slow scan speeds) to 64 minutes for a scan speed of 0.05 mm s^{-1}. Increasing the scan speed can further reduce the measurement time to 38 minutes for 0.1 mm s^{-1}, or even less for faster scan speeds. However, image resolution and reliability of the images should not be affected by the aspect of shortening the measurement time required for the experiments. Therefore, it is important to define the actual image quality, to effectively evaluate the result of faster scan speeds on image quality. Optical analysis of the images is often subjective, as it depends on the color scale used, the scaling method, and, of course, the eyes of the user. Therefore, conclusions drawn from this approach might be misleading and the interpretation of the results may not reveal the actual best measurement conditions. Figure 3a shows a distribution image of ^{65}Cu and Figure 3b shows the microscopic image of the very same pattern. The structure of the copper distribution on the printed areas appears to be very smooth and the edges are sharp; no blurring effects can easily be seen.

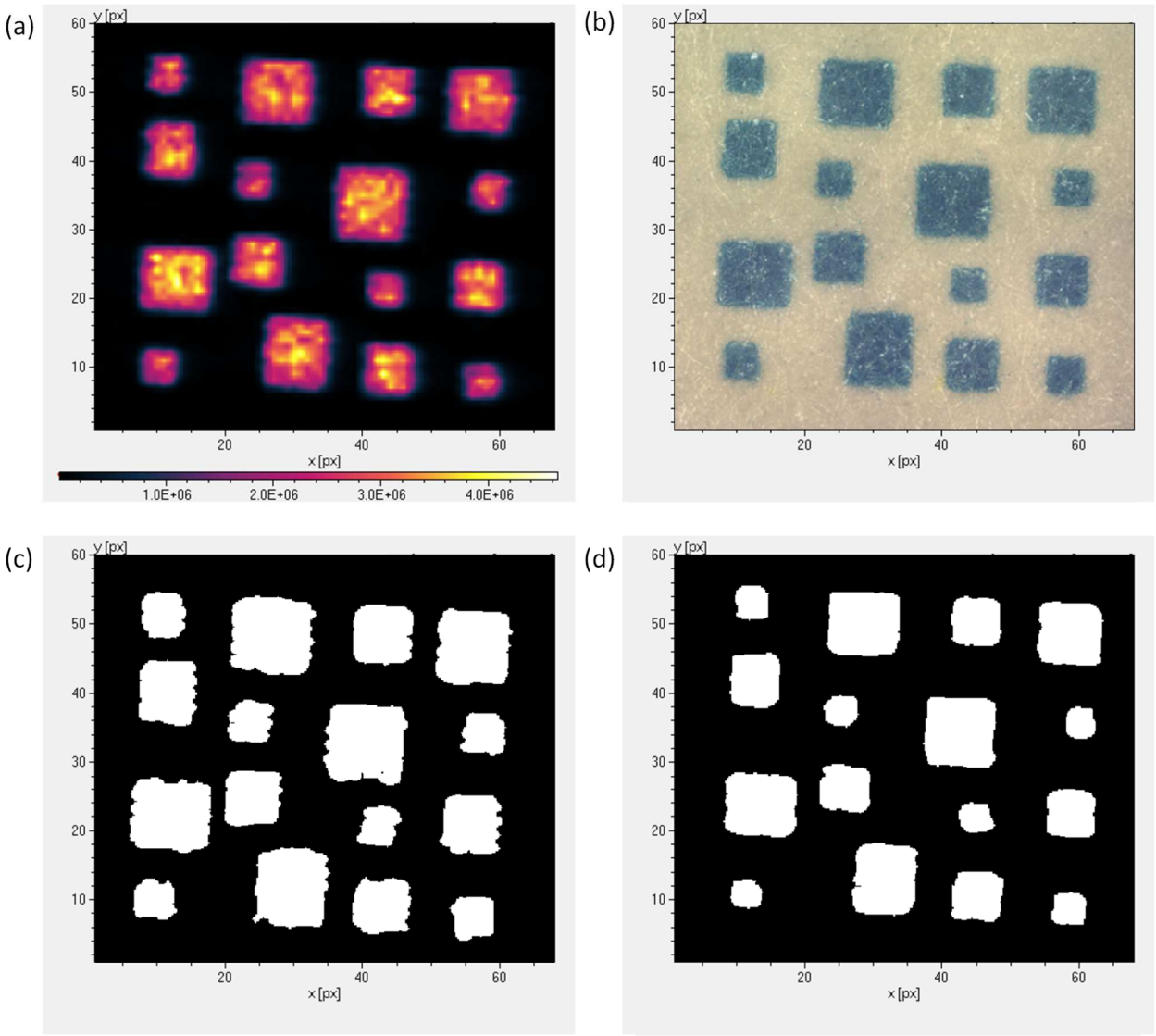

Figure 3: Elemental distribution of ^{65}Cu (a) and the microscopic image of the same pattern taken before sample analysis (b). LA-ICP-MS analysis was performed using a scan speed of 0.05 mm s^{-1} and a laser repetition rate of 40 Hz with the small washout cell. Elemental distribution (c) and visual image (d) after conversion to binary images.

However, the comparison of two or more images is very difficult and it is almost impossible to determine which one of a series of images represents the actual copper distribution better, and which measurement conditions should be preferentially used. The images are converted to binary images (Figure 3c and d). After subtraction of the two images, differences can be highlighted.

Subtraction of the visual image and the elemental distribution map

Visualization of the differences between the optical and the elemental image provides insight into the occurrence of mismatched areas. After image processing and construction of binary images the

individual pixel values of aligned images were subtracted. The results of selected samples are shown as difference images in Figure 4.

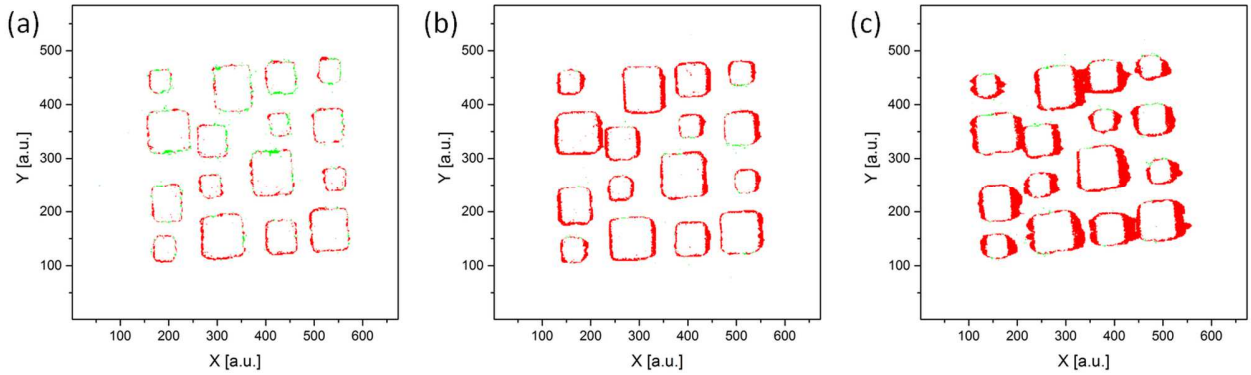

Figure 4: Difference plots of visual image and elemental distribution (^{65}Cu) for a spotscan (a) and linescans with 0.05 mm s^{-1} (b) and 0.2 mm s^{-1} scan speed (c) acquired at 40 Hz repetition rate using the large washout cell; red areas show ^{65}Cu signal above the threshold and do not have blue color (positive bias), green areas have blue color but the ^{65}Cu signal does not exceed the threshold (negative bias). The laser scan direction of all displayed images is from left to right.

The spotscan (Figure 4a) clearly shows the best accordance between the visual and elemental images, as only a minimal area is divergent between the visual and the chemical image of copper. Areas where copper is not present, but is detected above the threshold (red), and areas that contain copper, but none is detected (green) are relatively equal in amount and size. These areas mainly occur on the edges of the printed squares leading to the conclusion that shots might not hit areas with only ink or only paper and therefore lead to too low or too high signal intensities. This issue could be minimized using a higher lateral resolution (e.g. smaller laser beam diameters). In comparison, the linescan with low scan speed (Figure 4b) shows similar results. However, the edges are broader and most of the wrongly assigned areas represent overestimated copper signals. Especially in the scan direction (from left to right) the edges are wider, indicating slight blurring effects due to the material washout from the ablation cell. Still, the edges are sharp and the actual copper distribution is well represented in most of the image areas. The image with the high scan speed (Figure 4c) shows strong image blurring in scan direction and squares with less distance in between each other even become connected. This first step of the image analysis already reveals the differences between different sampling modes and measurement conditions. If the size of the wrongly assigned areas is set in relation to the overall image area, the area mismatch percentage (AMP) can be calculated.

Comparison of measurement conditions and washout cells

Using the proposed method for calculation of the wrongly assigned image area, measurement conditions and instrumental features can be compared. In the presented study, the method has been used to compare the following measurement conditions on the quality of the resulting elemental images of copper: laser repetition rate, scan speed, and two different cell volumes. An imaging experiment using a spotscan was considered as a reference value for the best obtainable image quality at a constant laser beam diameter; no image blurring will appear here. Sixteen measurement conditions were evaluated and applied to each of the two washout cells. This results in a total of 32 images measured using linescans. Furthermore, three images were measured with the same washout cell and the same experimental conditions, to evaluate the typical variation of the AMP value. This experiment was carried out using the large ablation cell and 0.1 mm s^{-1} scan speed at 20 Hz repetition rate. The average AMP

value of this series of experiments was 3.54 ± 0.13% indicating that the calculated percentages are very accurate. Even small variations may indicate significant changes in the quality of the resulting maps. A plot of the experimental conditions and the resulting AMP values is presented in Figure 5.

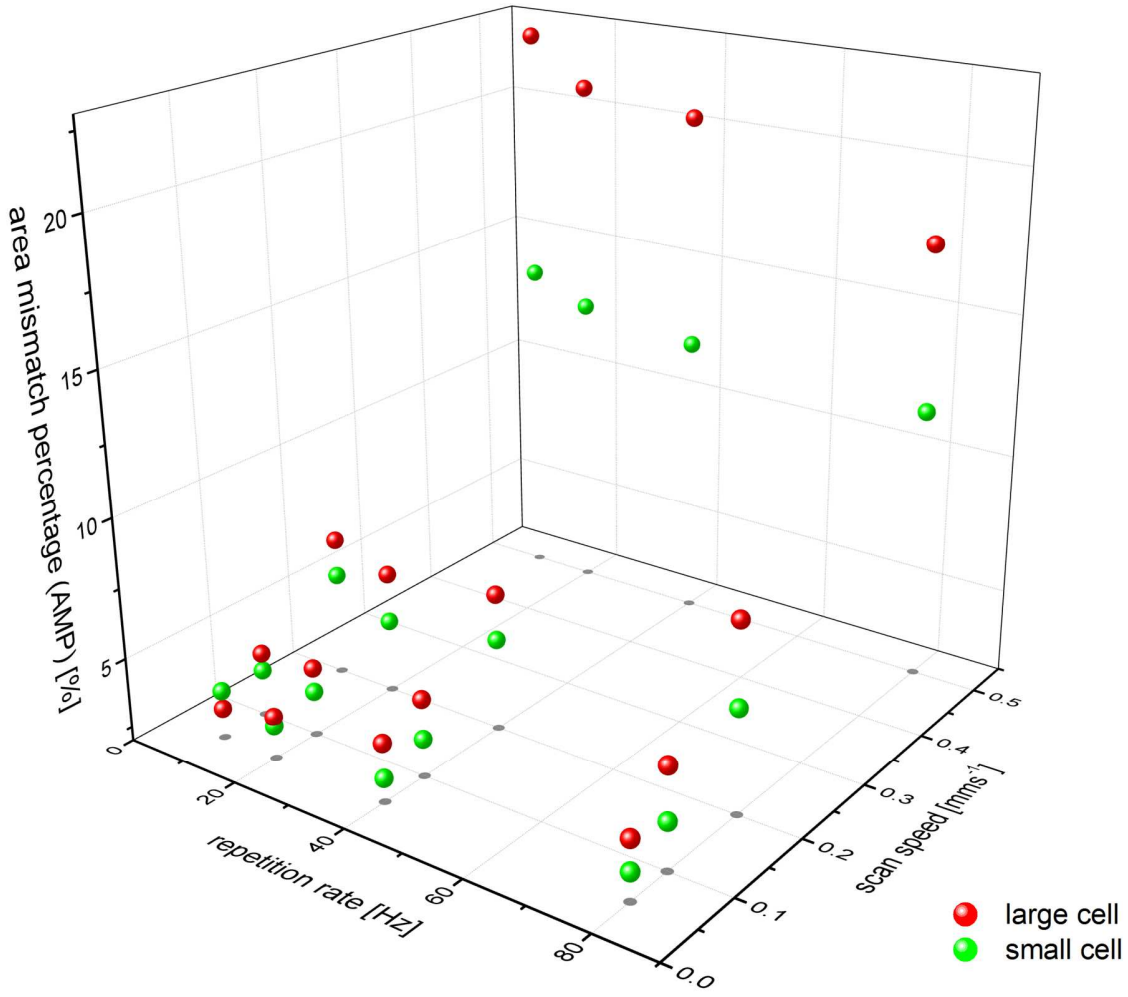

Figure 5: Area mismatch percentage (AMP) plotted against the experimental conditions using the large (red) and the small (green) aerosol washout cell

As demonstrated in Figure 4, higher scan speeds result in larger mismatched areas. This is reflected by the AMP values. Especially at scan speeds of 0.2 and 0.5 mm s^{-1}, the correlation of the visual image and the elemental map gets significantly worse compared to low scan speeds. The spotscan (measurement time: 12 h) has a lower AMP value (1.96%) than all linescans, showing that this approach results in the best image quality. The best AMP values with the linescan approach were achieved using the slowest scan speed and the small washout chamber, ranging between 2.5 and 3.0%. Comparing the two washout cells, the cell with the smaller volume shows overall lower AMP values. This gives the opportunity to use the same scan speed while improving image quality, or increasing the scan speed (shorter measurement time) while maintaining the same AMP value. For example, using a laser repetition rate of 80 Hz at a laser scan speed of 0.2 mm s^{-1} with the small washout cell will result in

almost the same AMP value (5.70%) as using the large cell at the same repetition rate and 0.1 mm s^{-1} (5.57%). However, this change reduces the measurement time from 38 min to 24 min. In contrast to changes of the scan speed, variation of the laser repetition rate only shows minor effects on the AMP value. Especially at higher scan speeds, results get slightly better with increased repetition rate. This might be attributed to the fact that the high repetition rate leads to faster complete material ablation, and ablated area overlap is reduced. However, if the whole sample material cannot be ablated, the repetition rate optimum might be found at a different value.

Conclusion

The proposed method for evaluation of image quality was shown to be a valuable approach to investigate sampling conditions in LA-ICP-MS imaging experiments. Printed patterns which can be reproducibly manufactured without major workload were used as model samples. As shown, the range of investigated analytes is not limited to elements that are typically constituents of ink[25]. The ink may be spiked with elements of interest in a concentration range that is expected to appear in the samples of interest. However, the washout behavior should not change dramatically between copper and other common metallic analytes. As the threshold values are calculated on a relative basis to the maximum of each measured image, variations in analyte concentration are not considered to be a major factor. Using this new approach, the image quality of the elemental distributions acquired using different experimental conditions and/or instrumentation can be compared on an objective basis. In future research, the effects of different image construction methods will be evaluated, which is also a current topic in the growing range of applications for LA-ICP-MS imaging.

Acknowledgment

The authors want to thank Applied Spectra, Inc. for providing access to instrumentation at their facility that was crucial for performing the experiments. M.B. wants to thank the MEIBio PhD program at the Vienna University of Technology for providing a scholarship over the period of 2013–2016. The research at LBNL was supported by the Chemical Science Division, Office of Basic Energy Sciences, U.S. Department of Energy under Contract No. DE-AC02-05CH11231.

1. R. E. Russo, X. Mao, J. J. Gonzalez, V. Zorba and J. Yoo, *Analytical chemistry*, 2013, **85**, 6162-6177. DOI: 10.1021/ac4005327.
2. D. Günther and B. Hattendorf, *TrAC Trends in Analytical Chemistry*, 2005, **24**, 255-265. DOI: http://dx.doi.org/10.1016/j.trac.2004.11.017.
3. J. Koch and D. Günther, *Applied spectroscopy*, 2011, **65**, 155-162. DOI: 10.1366/11-06255.
4. M. Thompson, J. E. Goulter and F. Sieper, *The Analyst*, 1981, **106**, 32-39. DOI: 10.1039/an9810600032.
5. J. J. Gonzalez, A. Fernandez, D. Oropeza, X. Mao and R. E. Russo, *Spectrochimica Acta - Part B Atomic Spectroscopy*, 2008, **63**, 277-286.
6. J. J. González, D. D. Oropeza, H. Longerich, X. Mao and R. E. Russo, *Journal of Analytical Atomic Spectrometry*, 2012, **27**, 1405-1412.
7. J. R. Chirinos, D. D. Oropeza, J. J. Gonzalez, H. Hou, M. Morey, V. Zorba and R. E. Russo, *Journal of Analytical Atomic Spectrometry*, 2014, **29**, 1292-1298.
8. B. Paul, J. D. Woodhead, C. Paton, J. M. Hergt, J. Hellstrom and C. A. Norris, *Geostandards and Geoanalytical Research*, 2014, **38**, 253-263.

9. P. Liu, F. Liu, C. Liu, J. Liu, F. Wang, L. Xiao, J. Cai and J. Shi, *Precambrian Research*, 2014, **246**, 334-357.
10. J. S. Becker, M. Zoriy, A. Matusch, B. Wu, D. Salber and C. Palm, *Mass spectrometry reviews*, 2010, **29**, 156-175. DOI: 10.1002/mas.20239.
11. C. Austin, D. Hare, A. L. Rozelle, W. H. Robinson, R. Grimm and P. Doble, *Metallomics : integrated biometal science*, 2009, **1**, 142-147. DOI: 10.1039/b901310p.
12. E. Moreno-Gordaliza, C. Giesen, A. Lazaro, D. Esteban-Fernandez, B. Humanes, B. Canas, U. Panne, A. Tejedor, N. Jakubowski and M. M. Gomez-Gomez, *Analytical chemistry*, 2011, **83**, 7933-7940. DOI: 10.1021/ac201933x.
13. O. Reifschneider, C. A. Wehe, I. Raj, J. Ehmcke, G. Ciarimboli, M. Sperling and U. Karst, *Metallomics : integrated biometal science*, 2013, **5**, 1440-1447. DOI: 10.1039/c3mt00147d.
14. M. A. da Silva and M. A. Arruda, *Metallomics : integrated biometal science*, 2013, **5**, 62-67. DOI: 10.1039/c2mt20154b.
15. K. M. Stika, C. S. Westphal, J. Kapur, R. G. Raty, J. Li, J. G. Kopchick, W. J. Gambogi, B. Hamzavytehrany, A. Z. Bradley, J. R. Marsh and B. W. Foltz, 2014 IEEE 40th Photovoltaic Specialist Conference, PVSC 2014.
16. C. Giesen, H. A. O. Wang, D. Schapiro, N. Zivanovic, A. Jacobs, B. Hattendorf, P. J. Schuffler, D. Grolimund, J. M. Buhmann, S. Brandt, Z. Varga, P. J. Wild, D. Gunther and B. Bodenmiller, *Nat Meth*, 2014, **11**, 417-422. DOI: 10.1038/nmeth.2869.
17. H. A. O. Wang, D. Grolimund, C. Giesen, C. N. Borca, J. R. H. Shaw-Stewart, B. Bodenmiller and D. Günther, *Analytical chemistry*, 2013. DOI: 10.1021/ac400996x.
18. D. Hare, B. Reedy, R. Grimm, S. Wilkins, I. Volitakis, J. L. George, R. A. Cherny, A. I. Bush, D. I. Finkelstein and P. Doble, *Metallomics : integrated biometal science*, 2009, **1**, 53-58. DOI: 10.1039/b816188g.
19. J. Lear, D. J. Hare, F. Fryer, P. A. Adlard, D. I. Finkelstein and P. A. Doble, *Analytical chemistry*, 2012, **84**, 6707-6714. DOI: 10.1021/ac301156f.
20. J. Lear, D. Hare, P. Adlard, D. Finkelstein and P. Doble, *Journal of Analytical Atomic Spectrometry*, 2012, **27**, 159-164. DOI: 10.1039/c1ja10301f.
21. D. J. Bellis and R. Santamaria-Fernandez, *Journal of Analytical Atomic Spectrometry*, 2010, **25**, 957-963. DOI: 10.1039/b926430b.
22. M. Bonta, H. Lohninger, M. Marchetti-Deschmann and A. Limbeck, *The Analyst*, 2014, **139**, 1521-1531. DOI: 10.1039/c3an01511d.
23. www.imagelab.at
24. A. D. McNaught and A. Wilkinson, *IUPAC. Compendium of Chemical Terminology, 2nd ed. (the "Gold Book")*, WileyBlackwell; 2nd Revised edition edition.
25. M. Bonta, H. Lohninger, V. Laszlo, B. Hegedus and A. Limbeck, *Journal of Analytical Atomic Spectrometry*, 2014, **29**, 2159-2167. DOI: 10.1039/C4JA00245H.